Citrate route to the piezoelectric $Pb(Zr,Ti)O_3$ oxide

Jin-Ho Choy* and Yang-Su Han

Department of Chemistry, Center for Molecular Catalysis, Seoul National University, Seoul 151-742, Korea

A homogeneous and stoichiometric $Pb(Zr_{1-x}Ti_x)O_3$ ($x=0.52$; PZT) powder with a particle size of 20–40 nm has been prepared by the citrate route. Solubility isotherms have been calculated for metal–citric acid–water systems at 25 °C to predict the optimum pH condition, which was found to be pH = 6.5 for preparing pure and stable citrate complexes. Monodispersive nanometer-sized particles could be obtained by thermal decomposition of the optimally prepared citrate precursor at a temperature as low as 800 °C. The crystallization process and particle characteristics of the citrate-derived PZT powder are described in detail along with the preliminary results on the sinterability and piezoelectricity.

$Pb(Zr,Ti)O_3$ (PZT) oxides, with ABO_3-type simple perovskite structure, are of interest because of their excellent ferroelectric, piezoelectric and the other electrical properties.[1,2] However, it is difficult to control the cation stoichiometry and particle size using the conventional solid-state reaction technique, because of the evaporation of PbO at high temperatures and long reaction times.[3–6] Such a method also leads to the formation of an undesirable intermediate phase and compositional fluctuation mainly in the morphotropic phase boundary (MPB) between tetragonal and rhombohedral phases.[7,8]

Alternatively, wet chemical routes to PZT *via* suitable precursors have attracted wide attention;[9–19] these allow a more homogeneous mixing of constituent cations, resulting in lowered processing temperature, higher reactive surface area, smaller particle size and narrower MPB. Among various chemical routes, alkoxide sol–gel[9–11] and coprecipitation[15–19] are the most well known. However, both are rather limited because of the difficulties in obtaining cationic solutions with similar solubility, in handling hygroscopic alkoxides and in controlling hydrolysis conditions precisely.

To overcome such limits, a sol–gel process using citrates, also called the Pechini method,[12,20] has been suggested for the preparation of fine particles with controlled stoichiometry. Since the mixing of constituent cations is carried out in the citrate solution, the resulting intermediate sol and gel retain their homogeneity during the process, which consequently results in the formation of fine reactive powders with the desired stoichiometry. However, the formation of a dense and rigid resin intermediate of citric acid and ethylene glycol, which requires extensive post-calcination grinding, is a problem in the original Pechini approach.[21,22] Moreover, an uncontrollable self-combustion of the intermediate resin during burning off of the organics leads to severe particle agglomeration in the calcined powders and causes the evaporation of volatile elements, especially PbO in lead-based oxide compounds, which results in the loss of cation stoichiometry. Taking this into account our primary attention was focused to the preparation of highly porous and soft intermediates in order to obtain fine PZT powders with no significant particle agglomeration. To do this, our citrate route utilizes only the chelating ability of the polyfunctional carboxylic acid (citric acid) without adding any esterification agents.

As previously pointed out,[23–25] the chelating ability of citric acid and the complexation reaction between metal ions and citric acid are highly dependent upon the solution pH, types and concentration of chemical species present in the solution. Thus, it is useful to investigate the chemical species present in the reaction system with respect to solution parameters for optimizing the preparation conditions of amorphous citrate precursors. In this work, we have carried out a simple but instructive theoretical investigation on solubility using only thermodynamic equilibrium constants to predict the behavior of various chemical species in aqueous solution. The present work is also concerned with the formation of nanometer-sized PZT powder from the amorphous citrate precursors and the characterization of citrate-derived PZT powders. Preliminary results on the sinterability and piezoelectricity of the citrate-derived PZT powders are also discussed briefly.

Theoretical solution modelling

The powder characteristics are highly dependent upon the chemical species present in the solution, and the nature of chemical species are also significantly influenced by solution variables such as pH, temperature, concentration, and so on.[23–28] From this point of view, solubility isotherms, which indicate the stability domains of various chemical species as a function of pH *vs.* metal ion concentration ($\log[M^{z+}]$), is very helpful in determining the optimum processing conditions.

Since the basic principles underlying the construction of solubility isotherms can be found in the literature,[29,30] details of numerical calculation are not included here. To establish solubility diagrams, well defined equilibrium reactions and their equilibrium constants are first needed and these are summarized in Table 1.[31–37] In solution where metal ions equilibrate with ligands, the species distribution is generally expressed as a function of ligand (citrate) concentration. However, it is more practical to express the species distribution as a function of pH since the hydroxide anion is always incorporated as a competing ligand in aqueous solution. We thus used pH instead of $[C_6H_5O_7^{3-}\ (L)]$ as a master variable to control the equilibrium reactions.

Dissociation of citric acid

Citric acid, $C_6H_8O_7$, is a weak triprotic acid, and dissociates in a stepwise manner in solution depending upon the pH as follows;

$$C_6H_8O_7\ [H_3L] = H^+ + C_6H_7O_7^-\qquad \log K_1 = -3.10$$

$$C_6H_7O_7^-\ [H_2L] = H^+ + C_6H_6O_7^{2-}\qquad \log K_2 = -4.80$$

$$C_6H_6O_7^{2-}\ [HL] = H^+ + C_6H_5O_7^{3-}\ [L]\qquad \log K_3 = -6.40$$

From the mass law and charge neutrality principle, the concentration of citrate (L) species can be given as follows;

$$[L] = \alpha_{[L]}A_T = [(K_1K_2K_3)/([H^+]^3 + K_1[H^+]^2 + K_1K_2[H^+] + K_1K_2K_3)]A_T \qquad (1)$$

where α_L is the ionization fraction of citrate anion, $C_6H_5O_7^{3-}$ (L), and A_T is the total concentration of citrate

Table 1 Chemical equilibria and their equilibrium constants

no.	equilibria	symbol[a]	log of constant	ref.
1	$C_6H_8O_7 = H^+ + C_6H_7O_7^-$	K_1	−3.10	31
2	$C_6H_7O_7^- = H^+ + C_6H_6O_7^{2-}$	K_2	−4.80	31
3	$C_6H_6O_7^{2-} = H^+ + C_6H_5O_7^{3-}$	K_3	−6.40	31
4	$Pb^{2+} + C_6H_5O_7^{3-} = Pb(C_6H_5O_7)^-$	β_1	4.10	31
5	$Pb^{2+} + 2C_6H_5O_7^{3-} = Pb(C_6H_5O_7)_2^{4-}$	β_2	6.10	31
6	$Pb^{2+} + C_6H_6O_7^{2-} = Pb(C_6H_6O_7)^0(aq)$	β_3	3.00	31
7	$Pb^{2+} + C_6H_7O_7^- = Pb(C_6H_7O_7)^+$	β_4	1.50	31
8	$Pb^{2+} + H_2O = Pb(OH)^+ + H^+$	β_1*	−7.71	32
9	$Pb^{2+} + 2H_2O = Pb(OH)_2^0(aq) + 3H^+$	β_2*	−17.01	32
10	$Pb^{2+} + 3H_2O = Pb(OH)_3^- + 3H^+$	β_3*	−28.06	32
11	$6Pb^{2+} + 8H_2O = Pb_6(OH)_8^{4+} + 8H^+$	β_6*	−43.6	32
12	$Pb(OH)_2(s) = Pb^{2+} + 2OH^-$	K_{sp}	−15.3	32
13	$Zr^{4+} + C_6H_5O_7^{3-} = Zr(C_6H_5O_7)^+$	β_1	8.00	33
14	$Zr^{4+} + 2C_6H_5O_7^{3-} = Zr(C_6H_5O_7)_2^{2-}$	β_2	14.00	33
15	$Zr^{4+} + C_6H_6O_7^{2-} = Zr(C_6H_6O_7)^{2+}$	β_3	10.80	33
16	$Zr^{4+} + H_2O = Zr(OH)^{3+} + H^+$	β_1*	0.30	32
17	$Zr^{4+} + 2H_2O = Zr(OH)_2^{2+} + 2H^+$	β_2*	−1.70	32
18	$Zr^{4+} + 3H_2O = Zr(OH)_3^+ + 3H^+$	β_3*	−5.10	32
19	$Zr^{4+} + 4H_2O = Zr(OH)_4^0(aq) + 4H^+$	β_4*	−9.70	32
20	$Zr^{4+} + 5H_2O = Zr(OH)_5^- + 5H^+$	β_5*	−16.00	32
21	$4Zr^{4+} + 8H_2O = Zr_4(OH)_8^{8+} + 8H^+$	β_{48}*	9.20	32
22	$Zr(OH)_4(s) = Zr^{4+} + 4OH^-$	K_{sp}	−52.0	34
23	$TiO^{2+} + C_6H_5O_7^{3-} = TiO(C_6H_5O_7)^-$	β_1	11.90	35
24	$TiO^{2+} + 2C_6H_5O_7^{3-} = TiO(C_6H_5O_7)_2^{4-}$	β_2	6.40	35
25	$TiO^{2+} + C_6H_7O_7^- = TiO(C_6H_7O_7)^+$	β_3	2.90	35
26	$TiO^{2+} + 2C_6H_7O_7^- = TiO(C_6H_7O_7)^0(aq)$	β_4	5.40	35
27	$TiO^{2+} + H_2O = TiO(OH)^+ + H^+$	β_1*	−1.60	36
28	$TiO^{2+} + 2H_2O = TiO(OH)_2^0(aq) + 2H^+$	β_2*	−4.10	36
29	$8TiO^{2+} + 12H_2O = TiO_8(OH)_{12}^{4+} + 12H^+$	β_{812}*	−1.70	36
30	$TiO^{2+} + H_2O_2 = TiO(H_2O_2)^{2+}$	K	−4.0	37
31	$TiO(OH)_2(s) = TiO^{2+} + 2OH^-$	K_{sp}	−27.9	36

[a] β* = Overall stability constants representing the protolytic equilibria; β = overall stability constant; K = normal stability constant; K_{sp} = solubility product.

($A_T = [H_3L] + [H_2L] + [HL] + [L]$) in mol dm^{-3}. Introducing the equilibrium constants and total concentration (1.0 mol dm^{-3} in this work), the concentrations of citrate species (log C_i) can be given as a function of pH as shown in Fig. 1. Four types of citrate species, H_3L, H_2L, HL, and L exist as the dominant species in the pH ranges of pH < 3.1 (pK_1), 3.1 (pK_2) < pH < 4.8 (pK_2), 4.8 (pK_2) < pH < 6.4 (pK_3) and pH > 6.4 (pK_3), respectively.

Solubility of the lead(II)–citric acid–water system

The numerical details used in constructing the solubility diagrams of metal citrates are given for the lead(II)–citric acid–water system as a model case. First, the most probable solid phase in the lead(II)–citric acid–water system is lead hydroxide, $Pb(OH)_2(s)$, and its solubility equilibrium is given by;

$$Pb(OH)_2(s) = Pb^{2+} + 2OH^- \qquad \log K_{sp} = -15.3 \qquad (2)$$

Rearranging eqn. (2) and taking logarithms,

$$\log [Pb^{2+}] = \log K_{sp} - 2 \log [OH^-] = 12.7 - 2pH \qquad (3)$$

Considering the hydrolysis of lead species using the equilibria in Table 1 (no. 8–11), the solubility isotherm of $Pb(OH)_2(s)$ in the pure lead(II)–water system can be obtained as shown in Fig. 2 by a thin solid line. This solid line denotes the total concentration of soluble lead species [C_T(Pb)] in equilibrium with $Pb(OH)_2(s)$ where $C_T(Pb) = [Pb^{2+}] + [Pb(OH)^+] + [Pb(OH)_2^0(aq)] + [Pb(OH)_3^-] + [Pb_6(OH)_8^{4+}]$. It is seen that the $Pb(OH)_2(s)$ begins to precipitate at pH = 8.4 from a

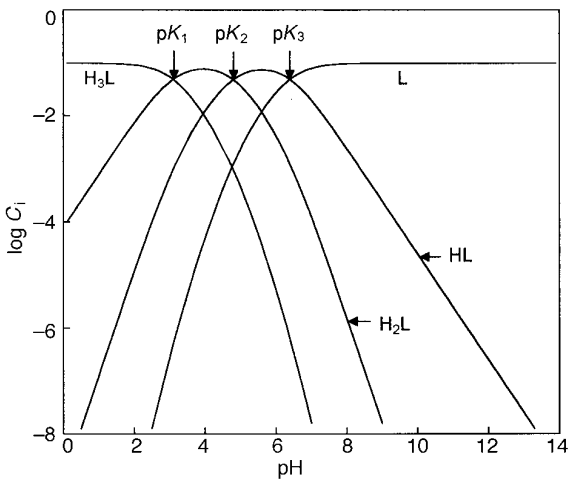

Fig. 1 Log C_i–pH diagram for a triprotic citric acid at 25 °C

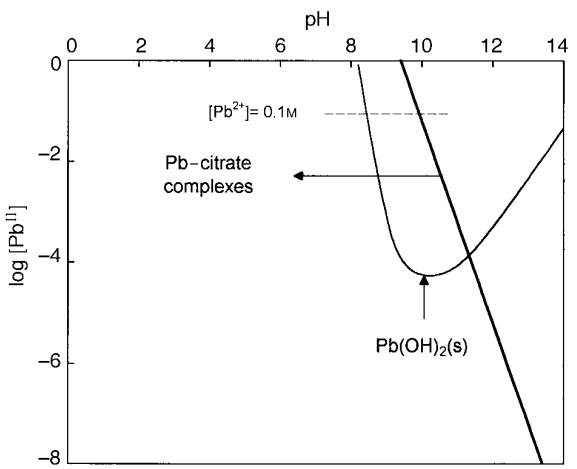

Fig. 2 Solubility isotherm of the Pb^{II}–citric acid–H_2O system at 25 °C

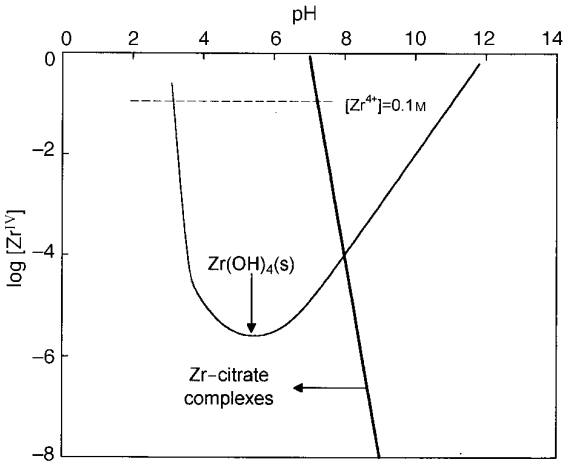

Fig. 3 Solubility isotherm of the Zr^{IV}–citric acid–H_2O system at 25 °C

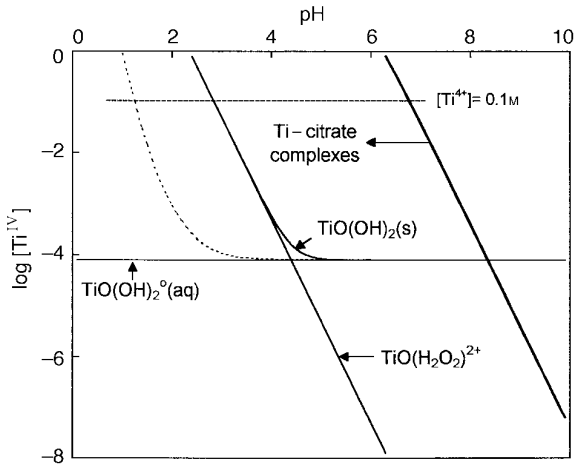

Fig. 4 Solubility isotherm of the Ti^{IV}–citric acid–H_2O system at 25 °C

solution containing 0.1 mol dm^{-3} Pb^{2+} and its solubility reaches a minimum at pH *ca.* 10.

Besides the hydrolysis equilibria, complexation due to citric acid becomes more significant in the lead(II)–citric acid–water system. The concentration of lead citrate complexes which equilibrate with $Pb(OH)_2$(s) can be estimated from the pertinent equilibria in Table 1 (no. 4–7), for example,

$$Pb^{2+} + C_6H_5O_7^{3-} = Pb(C_6H_5O_7)^- \qquad \log \beta_1 = 4.10 \quad (4)$$

Also, rearranging and taking logarithms,

$$\log[Pb(C_6H_5O_7)^-] = \log[Pb^{2+}] + \log \beta_1 + \log[C_6H_5O_7^{3}] \quad (5)$$

Introducing the β_1 value and substituting $\log[Pb^{2+}]$ in eqn. (3) and $\log[C_6H_5O_7^{3-}]$ in eqn. (1), the $Pb(C_6H_5O_7)^-$ concentration equilibrated with solid $Pb(OH)_2$(s) can be plotted *vs.* pH. The other citrates can also be considered similarly. For simplicity, only the total concentration of soluble lead citrates are shown in Fig. 2, where the thick solid line represents the total concentration of soluble citrates species in equilibrium with lead hydroxide, *i.e.*,

$$C_T(Pb) = [Pb(C_6H_5O_7)^-] + [Pb(C_6H_5O_7)_2^{4-}] + [Pb(C_6H_6O_7)^0(aq)] + [Pb(C_6H_7O_7)^+] \quad (6)$$

As the citrate anions take part in the complexation, the precipitation of lead hydroxide is suppressed until the pH value reaches *ca.* 10 owing to the formation soluble citrate complexes. In other words, stable lead citrate complexes can be formed below a solution pH = 10.

Solubility of the zirconium(IV)–citric acid–water system

The possible chemical species in the zirconium(IV)–citric acid–water system and their equilibrium constants are listed in Table 1 and the solubility curves obtained are plotted as a function of pH in Fig. 3. For comparison, the solubility curve of $Zr(OH)_4$(s) is also overlapped in this figure. The precipitation of $Zr(OH)_4$(s) in the absence of citric acid begins at low pH (pH *ca.* 3) because of the strong hydrolysis tendency of Zr^{4+}. Since Zr^{4+} has a higher charge-to-size ratio than Pb^{2+}, the hydrolysis effect on the solubility is more significant for Zr than for Pb. However, $Zr(OH)_4$(s) precipitation is strongly suppressed in the presence of the citric acid complexing agent. Hydroxide precipitation can occur above pH = 7 when $[Zr^{4+}] = 0.1$ mol dm^{-3}. The thick solid line represents the total concentration of the soluble zirconium citrates;

$$C_T(Zr) = [Zr(C_6H_5O_7)^+] + [Zr(C_6H_5O_7)_2^{2-}] + [Zr(C_6H_7O_7)^{2+}] \quad (7)$$

Below pH = 7, such zirconium citrates exist as predominant species rather than hydroxy complexes.

Solubility of the titanium(IV)–citric acid–water system

In the titanium(IV)–citric acid–water system, titanium hydroxide, $TiO(OH)_2$(s), is most likely to precipitate as a solid phase. In aqueous solution, Ti^{4+} [or $Ti(OH)^{2+}$, TiO^{2+}] is rapidly hydrolyzed and precipitated as $Ti(OH)_4$ [or $TiO(OH)_2$(s)] owing to its high size-to-charge ratio. In general, hydrogen peroxide, which strongly forms complexes with the Ti^{4+} ion, is added to suppress the hydrolytic precipitation of TiO_2. The effect of H_2O_2 on the solubility of $TiO(OH)_2$(s) can be seen clearly in Fig. 4. In the absence of H_2O_2 (dotted line), $TiO(OH)_2$(s) precipitates immediately at pH = 1, which shifts to pH = 3 in the presence of H_2O_2 owing to the formation of a soluble $TiO(H_2O_2)^{2+}$ complex. When citric acid competitively takes part in the complex formation reaction, the titanium citrate complexes dominate at pH < 7 while the precipitation of $TiO(OH)_2$(s) becomes possible beyond pH = 7. Therefore, the distribution of dominant soluble species with respect to pH can be expected as follows; titanium citrates such as $TiO(C_6H_5O_7)_2^{4-}$ at pH < 8 and $TiO(OH)_2^0$(aq) at pH > 8, respectively.

Solubility of the lead(II)–zirconium(IV)–titanium(IV)–citric acid–water system

We can now estimate the optimum pH value for preparing a stable PZT–citrate precursor based on the solubility curves of individual metal citrates. According to Fig. 2, the pH range of < 10 seems to be suitable for the formation of stable lead citrate complexes without interference of hydroxide precipitation. Stable citrate complexes for zirconium and titanium are formed below pH < 7 (Fig. 3 and 4) without competing hydroxide precipitation which leads to the segregation of the component metal ions. Finally, pH > 6.4 (pK_3) favors maximization of ionization of citric acid (Fig. 1). As a consequence, it can be concluded that the solution pH should be controlled to pH ≈ 6.5 to obtain a homogeneous and stoichiometric PZT–citrate precursor.

Experimental

Powder preparation

The starting reagents used were high purity $Pb(NO_3)_2$, $TiCl_4$ and $ZrOCl_2 \cdot 8H_2O$. In preparing the source solution of

titanium, titanium tetrachloride was dissolved in a 30% H_2O_2 aqueous solution to prevent hydrolytic precipitation of titanium hydroxide, then the titanium content was determined volumetrically,[28] and diluted to give a 0.1 mol dm^{-3} aqueous solution. $Pb(NO_3)_2$ and $ZrOCl_2 \cdot 8H_2O$ were also dissolved in distilled water and also diluted to 0.1 mol dm^{-3}. A schematic diagram for preparing PZT powders by the citrate route is shown in Fig. 5. To prepare Pb, Zr and Ti aqueous citrate solutions, a weighed quantity of citric acid ($C_6H_8O_7 \cdot 2H_2O$), which corresponds to a 1.0 mol dm^{-3} citrate solution, was added to each aqueous solution. Then the aqueous citrate solutions were intermixed in a mole ratio $Pb(Zr_{0.52}Ti_{0.48})O_3$. After mixing the solution pH was raised to 6.5 by adding 30% ammonia solution. Upon evaporating the water slowly from the solution at 80 °C, a colorless colloidal suspension was initially formed. Further heating for 1–2 h at 100–150 °C resulted in dark-colored, amorphous citrate gels with high viscosity, which were then subjected to calcination at various temperatures for 2 h.

Powder characterization

Thermolysis of the amorphous citrate precursor was examined under an ambient atmosphere by simultaneous thermogravimetry (TG) and differential scanning calorimetry (DSC) with a Rigaku thermal analyzer (TAS-100) from room temperature to 800 °C (heating rate = 10 °C min^{-1}). Crystalline phase evolution of calcined powders was monitored by powder X-ray diffraction (Philips PW-1830) using Ni-filtered Cu-Kα radiation ($\lambda = 1.5418$ Å). Specific surface areas of powders calcined at 800 °C were determined by a conventional three-point BET technique at liquid-nitrogen temperature with Quantasorb. Average particle sizes and morphologies of selected calcined PZT powders and sintered specimens were examined by scanning electron microscopy (SEM) (JSM-8404). Inductively coupled plasma (ICP) (Shimazu ICPS-5000) analysis was also performed to determine the cation stoichiometry of calcined PZT samples.

Sintering and piezoelectric property measurements

The citrate-derived PZT powders calcined at 800 °C for 2 h were sintered at different temperatures between 1050–1200 °C for 2 h. A buffer PbO atmosphere was not used during the sintering. For sintered samples, the apparent density was measured geometrically and the microstructure was observed by SEM on freshly fractured surfaces.

For measuring piezoelectric properties, the sintered specimens were polished, electroded and then poled in a silicon oil bath by applying a dc electric field of 3.5 kV mm^{-1} at 100 °C for 30 min. After poling, the specimens were aged for 24 h prior to measuring the dielectric and piezoelectric properties. The piezoelectric parameters were determined by the resonance method following IRE standards at 1 kHz.[38] The piezoelectric coefficient d_{33} of the samples was measured using a Berlincourt Piezo-d_{33} meter.

Results and Discussion

The Pechini process[20] involves the ability of certain weak acids to form polybasic acid chelates with various cations. These chelates can undergo polyesterification when heated in polyhydroxy alcohols (usually ethylene glycol), which is added to aid dissolving metal salts, to form a resin intermediate. However a resin intermediate with superfluous organic groups usually bursts into flames during calcination. This uncontrollable burning leads to undesirable particle agglomeration and PbO evaporation. It is, therefore, recommended to reduce the organic content as much as possible.

Citric acid used in this study as a chelating agent strongly complexes with metal ions and the metal citrate complexes tend to be fairly stable if the solution conditions are properly controlled. According to the solubility isotherms (Fig. 1–4), formation of pure and stable citrate complexes was found at pH = 6.5. By adjusting the pH to this value after mixing the constituent solutions, we could obtain a clear metal citrate sol, which enabled successful polymerization to occur without the addition of any esterification agent.

Thermal analysis

To understand the thermal behavior of the citrate gel precursors, simultaneous TG–DSC plots were recorded at a constant heating rate of 10 °C min^{-1} up to 800 °C as shown in Fig. 6. Three distinct exothermic peaks in the temperature range 350–600 °C are visible in the DSC curve together with a drastic mass loss in the TG curve, which can be assigned to the oxidative decomposition of citrates.[26] This amorphous citrate does not show any high-temperature mass loss, indicating the formation of the PZT lattice prior to the vaporization of PbO.

Crystallization of PZT

The powder X-ray diffraction patterns for the citrate gel precursor (a) and the products calcined at 600 °C (b) and 800 °C (c) for 2 h are shown in Fig. 7. The obtained citrate

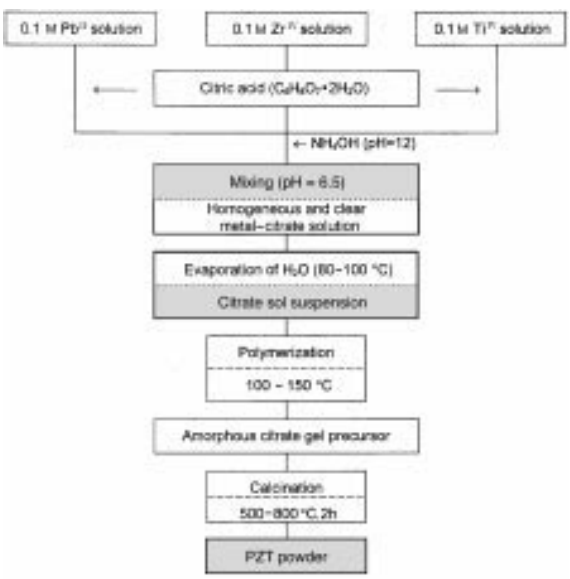

Fig. 5 Schematic diagram for the $Pb(Zr_{0.52}Ti_{0.48})O_3$ powder preparation using the amorphous citrate route

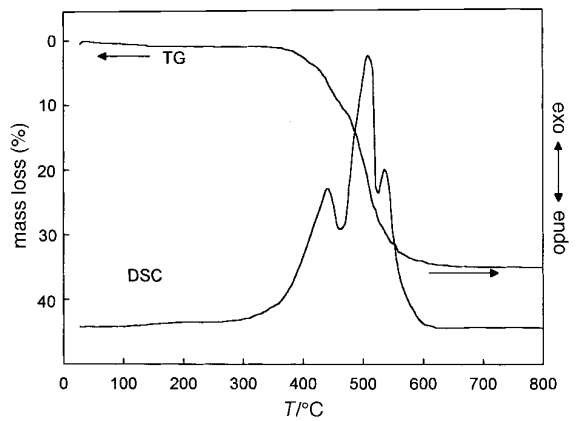

Fig. 6 TG–DSC curves of the PZT–citrate precursor under ambient atmosphere with a heating rate of 10 °C min^{-1}

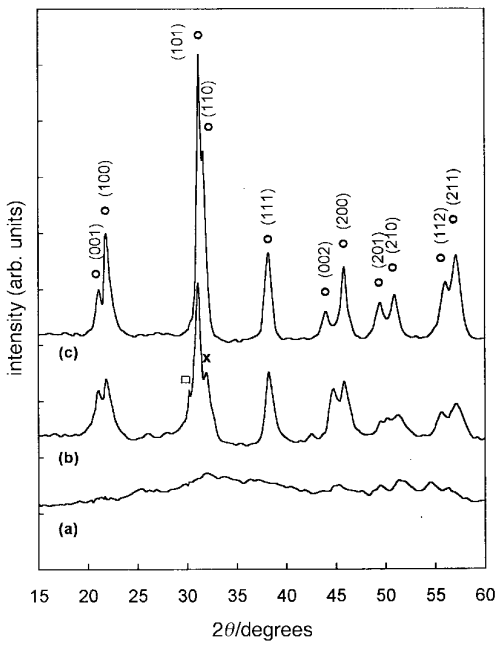

Fig. 7 Powder X-ray diffraction patterns for the calcined PZT powders at the given temperature for 2 h. (a) Precursor, (b) 600 °C, (c) 800 °C; ○, PZT; ×, $PbTiO_3$; □, $PbZrO_3$.

precursor is amorphous up to 600 °C at which point the decomposition of organics is complete and crystallization of PZT starts to take place. A monophasic PZT phase could be obtained after calcination at 800 °C, which is quite low compared to the temperatures required in the solid-state reaction (*ca.* 1000 °C). The faster formation of the monophasic PZT phase in our citrate process is due to the higher degree of compositional homogeneity and larger reactive surface area of the citrate-derived PZT precursor powder. All the reflection patterns can be indexed to tetragonal symmetry ($a=4.016$ Å, $c=4.110$ Å) corresponding to the composition $Pb(Zr_{0.52}Ti_{0.48})O_3$. The absence of a rhombohedral phase suggests the homogeneous distribution of Ti^{4+} and Zr^{4+} in B-sites of the perovskite lattice.[2,4,5]

Particle characteristics

A scanning electron micrograph of the citrate-derived PZT powder calcined at 800 °C is shown in Fig. 8 and the particle characteristics of the citrate-derived PZT powder are summarized in Table 2. As can be seen from the SEM photograph, the

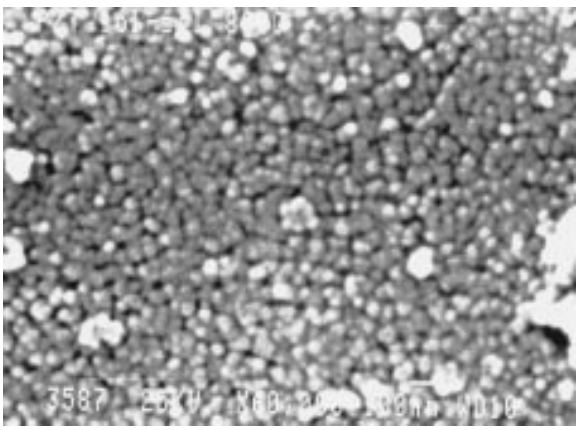

Fig. 8 Scanning electron micrograph of the citrate-derived PZT powder calcined at 800 °C for 2 h

Table 2 Characteristics of the citrate-derived PZT powder

particle morphology	spherical
particle size/nm (SEM)	20–40
specific surface area/$m^2\ g^{-1}$ (BET)	37
ESD[a]/nm	≈20
crystallite size[b]/nm	≈21
cation stoichiometry[c]	$Pb_{0.989}(Zr_{0.520}Ti_{0.482})O_3$

[a]ESD = Equivalent spherical diameter calculated from surface area; $d=6/S_{BET}\rho$ where S_{BET} = specific surface area ($m^2\ g^{-1}$) and ρ = theoretical density of PZT (8.147 g cm^{-3}). [b]Estimated from X-ray line broadening effect using Scherrer formula $t=0.9\lambda/B\cos\theta$ where t = diameter of crystallite, B = broadening of diffraction lines (radians) and λ = wavelength (1.5418 Å). [c]Determined by inductively coupled plasma (ICP) analysis.

citrate-derived PZT powders consist of fine spherical and monodispersed particles. The particle sizes are estimated to be in the range 20–40 nm, much finer than previously reported. X-Ray peak broadening indicates that the primary crystallite size is *ca.* 21 nm. The BET surface area reveals that the powder has a large reactive surface area of *ca.* 37 $m^2\ g^{-1}$. The equivalent spherical diameter (ESD) calculated from the surface area is *ca.* 20 nm, which is in excellent agreement with the value estimated from the X-ray line-broadening effect. Comparison of the particle sizes estimated from SEM, BET and X-ray line broadening indicates that the calcined PZT powders are composed of almost monodisperse nanometer-sized particles. Such a result confirms that our amorphous citrate route is quite effective for producing non-agglomerated fine particles by avoiding the use of organics such as ethylene glycol. Elemental analysis (Table 2) indicates that the overall cation stoichiometry is retained almost completely during the PZT crystallization. The metal cations in the sol state retain their homogeneity during gelation, and cations captured in the citrate gel matrix readily react with each other to form the stoichiometric PZT phase upon calcination.

Sinterability and piezoelectric properties

In order to study the sinterability of the citrate-derived PZT powders, the bulk density of the samples was measured as a function of sintering temperature as plotted in Fig. 9. The bulk density increases rapidly and reaches a maximum (94%) at 1100 °C, and then reduces with further increase in temperature. The large reactive surface area of the citrate-derived PZT powder exerts a high driving force for sintering, thereby leading to enhanced densification at a temperature as low as 1100 °C.

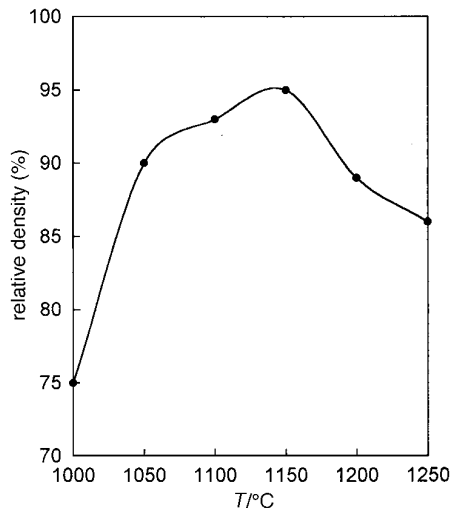

Fig. 9 Relative density of the sintered PZT specimens as a function of temperature

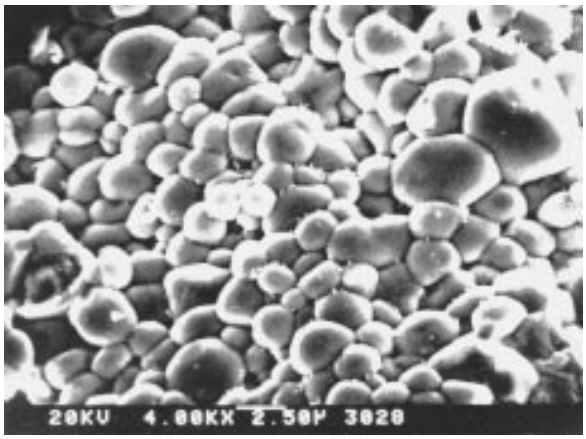

Fig. 10 Scanning electron micrograph on the freshly fractured surfaces of PZT sample sintered at 1100 °C for 2 h

Table 3 Sinterability and piezoelectric properties of sintered PZT sample

dissipation factor/tanδ	0.029
electromechanical coupling coefficient/K_p	0.42
mechanical quality factor/Q_m	70
relative permittivity/ε_{33}^T(at 1 kHz)	310
piezolectric constant/d_{33}	141

A decrease in bulk density above 1200 °C might be attributed to a rapid material flow originating from high surface activity of the citrate-derived PZT powders, leading to the formation of internal (closed) pores in sintered specimens and subsequent pore coarsening. Fig. 10 shows a scanning electron micrograph on the fractured surfaces of a specimen sintered at 1100 °C. The sintered sample consists of fine and comparatively uniform grains of size 2–5 μm with spherical morphology.

Table 3 summarizes the electrical characteristics for the sample sintered at 1100 °C. The piezoelectric properties of the citrate-derived PZT specimen are comparable to those of samples prepared previously.[1] Despite the excellent powder characteristics and sinterability, the electrical properties were not improved significantly, probably due to the effect of isotropic grain shape, which is responsible for lowering the dielectric and piezoelectric properties. Generally, dielectric and piezoelectric parameters are proportional to the remanent polarization, which is closely related to the grain shape in the sintered samples and is low for nearly spherical particles (Fig. 10).

Conclusions

Homogeneous and nanometer-sized PZT powders with high surface area (*ca.* 37 m^2 g^{-1}) have been prepared by the citrate route. The optimum pH condition (pH = 6.5) for the formation of pure and stable metal citrate complexes was estimated based on the theoretical consideration of solubility isotherms, which allow us to perform the polymerization reaction without adding any esterification additive such as ethylene glycol. A monophasic PZT powder with good compositional and structural homogeneity was obtained by thermal decomposition of amorphous PZT-citrate precursor at a temperature as low as 800 °C. The citrate-derived PZT powder was composed of nanometer-sized (20–40 nm) monodispersive particles and exhibited enhanced sinterability at a temperature as low as 1100 °C.

This work was in part supported by the Ministry of Science and Technology in the scope of the international cooperation and by the Korea Science and Engineering Foundation through the Center for Molecular Catalysis.

References

1 B. Jaffe, W. R. Cook and H. Jaffe, *Piezoelectric Ceramics*, Academic Press, New York, 1971.
2 K. Okazaki, *Ferroelectrics*, 1982, **41**, 77.
3 D. L. Hankey and J. V. Biggers, *J. Am. Ceram. Soc*., 1981, **64**, 172.
4 K. Kakegawa, J. Mohri, S. Shirasaki and K. Takahashi, *J. Am. Ceram. Soc*., 1982, **65**, 515.
5 R. R. Krishnan and P. Ramakrishnan, *Br. Ceram. Trans. J*., 1988, **87**, 99.
6 T. R. Shrout, P. Papet, S. Kim and G. S. Lee, *J. Am. Ceram. Soc*., 1990, **73**, 1862.
7 K. Kakegawa, J. Mohri, T. Takahashi, H. Yamamura and S. Shirasaki, *Solid State Commun*., 1977, **24**, 769.
8 S. A. Mabud, *J. Appl. Crystallogr*., 1980, **13**, 211.
9 T. Fukui, C. Sakurai and M. Okuyama, *J. Mater. Res*., 1992, **7**, 791.
10 N. Okada, K. Ishikawa, K. Murakami, T. Nomura, M. Hagino, N. Nishino and U. Kihara, *Jpn. J. Appl. Phys*., 1992, **31**, 304.
11 C. D. Chandler, C. Roger and M. J. Hampden-Smith, *Chem. Rev*., 1993, **93**, 1205.
12 R. Lal, R. Krishnan and P. Ramakrishinan, *Mater. Sci. Eng*., 1987, **96**, L25.
13 R. Lal, N. M. Gokhale, R. Krishnan and P. Ramakrishinan, *J. Mater. Sci*., 1989, **24**, 2911.
14 M. A. Zaghete, C. O. P. Santos, J. A. Varela, E. Longo and Y. P. Mascarenhas, *J. Am. Ceram. Soc*., 1992, **75**, 2088.
15 V. R. Palkar and M. S. Multani, *Mater. Res. Bull*., 1979, **14**, 1353.
16 T. R. N. Kutty and R. Balachandran, *Mater. Res. Bull*., 1984, **19**, 1479.
17 A. P. Singh, S. K. Mishra, D. Pandey, C. D. Prasad and R. Lal, *J. Mater. Sci*., 1993, **28**, 5050.
18 R. Balachandran and T. R. N. Kutly, *Mater. Chem. Phys*., 1984, **10**, 287.
19 H. Yamamura, S. Kuramoto, H. Haneda, A. Watanabe and S. Shirasaki, *J. Ceram. Soc. Jpn*., 1986, **92**, 470.
20 M. P. Pechini, *US Pat*., 3 330 697, July, 11, 1967.
21 L. W. Tai and P. A. Lessing, *J. Mater. Res*., 1992, **7**, 502.
22 L. W. Tai and P. A. Lessing, *J. Mater. Res*., 1992, **7**, 511.
23 J. H. Choy, Y. S. Han, S. W. Song and S. H. Chang, *J. Mater. Chem*., 1994, **4**, 1271.
24 J. H. Choy, Y. S. Han and Y. H. Kim, *Mater. Lett*., 1993, **16**, 226.
25 J. H. Choy, Y. S. Han and S. W. Song, *Mater. Lett*., 1994, **19**, 257.
26 J. H. Choy, Y. S. Han, J. T. Kim and Y. H. Kim, *J. Mater. Chem*., 1995, **5**, 57.
27 J. H. Choy, Y. S. Han, Y. H. Kim and K. S. Suh, *Jpn. J. Appl. Phys*., 1993, **32**, 1154.
28 J. H. Choy, Y. S. Han and J. T. Kim, *J. Mater. Chem*., 1995, **5**, 65.
29 F. M. M. Morel, *Principles of Aquatic Chemistry*, John Wiley & Sons, New York, 1983.
30 S. Morgan, *Aquatic Chemistry*, John Wiley & Sons, New York, 1983.
31 A. E. Martell and R. M. Smith, *Critical Stability Constants*, Plenum Press, New York, vol. 3, 1977.
32 C. F. Baes and R. E. Mesmer, *The Hydrolysis of Cations*, Wiley & Sons, New York, 2nd edn., 1976.
33 N. G. Strizhakova, *Ukr. Khim. Zh*., 1978, **44**, 227.
34 H. Bilinski, M. Branica and L. G. Sillen, *Acta Chem. Scand*., 1966, **20**, 853.
35 V. K. Zolotkhin, *Zh. Neorg. Khim*., 1973, **18**, 276.
36 H. Einaga, *J. Inorg. Nucl. Chem*., 1981, **43**, 2443.
37 E. Hogfeldt, *Stability Constants of Metal Ion Complexes, Part A. Inorganic Ligands*, IUPAC chemical data series, No. 21, Pergamon Press, New York, 1989.
38 H. Jaffe, *IRE Proc*., 1961, 1161.

Paper 7/00687J; *Received* 30*th January*, 1997